Supporting Information

Enhanced nano-scale Ge concentration oscillations in Si/SiGe quantum well through controlled segregation

Kevin-P. Gradwohl,*† Lukas Cvitkovich,‡ Chen-Hsun Lu,† Sebastian Koelling,¶ Maximilian Oezkent,† Yujia Liu,† Dominic Waldhör,‡ Tibor Grasser,‡ Yann-Michel Niquet,§ Martin Albrecht,† Carsten Richter,† Oussama Moutanabbir,¶ and Jens Martin†

† Leibniz-Institut für Kristallzüchtung, 12489 Berlin, Germany
‡ Institute for Microelectronics, Technische Universität Wien, 1040 Vienna, Austria
¶ École Polytechnique de Montréal, Montréal, H3T 1J4 Québec, Canada
§ Univ. Grenoble Alpes, CEA, IRIG-MEM-L Sim, F-38000 Grenoble, France

E-mail: kevin-peter.gradwohl@ikz-berlin.de
Phone: +49 (0)30 6392 3021
Fax: +49 (0)30 6392 3003

1 Experimental

1.1 Materials

$^{28}Si_{0.7}Ge_{0.3}/^{28}Si/^{28}Si_{0.7}Ge_{0.3}$ heterostructures were grown by MBE on fully-relaxed $Si_{0.7}Ge_{0.3}$ virtual substrates on Si. Isotopically enriched ^{28}Si solid source material from the Avogadro project with a ^{29}Si concentration below 30 ppm and a high chemical purity (C, O < 10^{16} cm^{-3}) was employed. This work employed natural Ge, but MBE growth with isotopically enriched Ge for nuclear spin-free WQWs is planned. The C and O concentrations in the grown heterostructures are <10^{18} cm^{-3}, as indicated by the APT data. The final constant composition $Si_{0.7}Ge_{0.3}$ layer of the virtual substrates (strain-relaxed buffers) has a moderate threading dislocation density of low 10^5 cm^{-2} and is capped with a 5 nm thick Si layer (Si cap) for controlled ex-situ cleaning. A standard Si wet-chemical cleaning procedure was utilized; involving degreasing for 5 minutes in acetone and isopropanol, 10 minutes in hot Piranha solution, 5 minutes in 0.5% HF solution, and a dip in deionized water. After the cleaning, the substrates were loaded into the load-lock chamber of the ultra-high vacuum system (10^{-10} mbar base pressure) with less than a minute of air exposure. In-situ annealing at 700°C for 10 minutes in vacuum and for 5 minutes including atomic hydrogen exposure at $3 \cdot 10^{-7}$ mbar was executed to get rid of most oxygen and carbon interface contamination. However, some overgrown carbon clusters at the interface could be detected by APT. The MBE-grown $^{28}Si_{0.7}Ge_{0.3}$ barrier was grown at 500°C, with varying temperatures for the WQW. Low evaporation rates for WQW growth were realized for the modulation of the growth temperature, not exceeding growth rates of 0.001 nm/s, allowing for the suppression of Ge segregation.

1.2 Characterization

1.2.1 STEM

We used Gatan's Precision Ion Polishing System (PIPS) to prepare the cross-sectional sample for STEM. Specifically, film sides of two heterostructures were glued together and mechanically polished down to a thickness of 10 µm using a series of diamond abrasive films with decreasing grain size prior to ion beam milling. The Ar ion guns in the PIPS were set to incident angles of ±5° and an accelerating voltage of 3 kV. The sample was thinned in the PIPS to electron transparency from both sides simultaneously. Finally, an acceleration voltage of 0.2 kV was used to remove the amorphous region created during ion beam milling.

The STEM investigations were carried out using an aberration corrected FEI Titan 80-300 TEM, operated at 300 kV. The angular range for the ADF detector collection was nominally 36-150 mrad. Atomic-resolution ADF-STEM images were captured along the [110] zone axis. To analyse the concentration profile, the original intensity was adjusted in post-processing to account for the thickness change in the wedge-shaped sample along the epitaxial direction, which is assumed to decrease quadratically.

1.2.2 APT

Atom Probe Tomography samples were prepared in a FEI Helios Nanolab 660 dualbeam scanning electron microscope using a gallium-focused ion beam (FIB) at 30, 16, and 5 kV. A 120-150 nm-thick chromium capping layer was deposited in a thermal evaporator before the FIB preparation to limit the implantation of gallium into the region imaged during APT. APT analyses were carried out in a LEAP 5000XS tool utilizing a picosecond laser to generate laser pulses at a wavelength of 355 nm. During the analyses, samples were cooled to a base temperature of 25 K before laser pulses with an energy of 8-10 pJ were applied to assist with field evaporation.

1.3 Simulation

The valley splittings that can be expected from the heterostructures presented in this work are calculated by means of a sp3d5s* TB model implemented in TB_Sim.[26] The periodic supercell consists of 24×24 conventional Si unit cells in plane and 50 unit cells in growth direction summing up to a total of 230400 atoms. The dimensions are 13.2×13.2×27.3 nm^3. The well width is 10 nm and the oscillating Ge concentrations are defined by the averaged Ge content in each monolayer. Within each monolayer, Si atoms are randomly replaced with Ge until the Ge distribution follows the desired Ge profile. The structures are then relaxed using a Valence Force Field.[26,27] We apply a periodic sawtooth potential to the heterostructure, with an electric field E_z = 5 mV/nm in the well (a typical value for gate-confined quantum dots in Si/SiGe) and E_z = -2.9 mV/nm in the barrier. The valley splitting of 50 random configurations of Ge atoms is simulated for each nominal Ge profile and depicted in a box plot.

2 Complementary Experiments

2.1 Molecular Beam Epitaxy (MBE) Test structures

An exemplary wiggle quantum well (WQW) test structure can be seen in Fig. S1a. After surface preparation and in-situ annealing of the substrates, 30 nm $^{28}Si_{0.7}{}^{nat}Ge_{0.3}$ was grown at 500°C, followed by a strained Si layer with 15 Ge oscillations, followed by a 5 nm $^{28}Si_{0.7}{}^{nat}Ge_{0.3}$ cladding layer. A growth temperature of 500°C was necessary to achieve a good surface morphology. Growth below 450°C yielded roughening and growth at 350°C already a slight onset of pit formation.

The respective transmission electron microscopy (TEM) contrast profile is depicted in Fig. S1b. After five subsequent Ge oscillations the shutter control and configuration were changed to demonstrate the effects of Ge segregation during epitaxy. The first set of five Ge concentration oscillations (I) were grown at 450°C by keeping the Si shutter open for 45 s with the Ge shutter closed, followed by both shutters being open for 30 s, for each period. The Si and Ge growth rate were kept constant at 0.02 nm/s and 0.0086 nm/s, respectively. The next five Ge oscillations (II) were grown at 500°C, but with the shutter configuration and growth rates of (I). The last five Ge concentration oscillations (III) were grown at 500°C with both the Si and Ge shutter open, while keeping the Si growth rate constant at 0.01 nm/s and oscillating the Ge evaporation rate between 0 and 0.002 nm/s with a period time of 170 s, which is the limit of the maximal possible heating and cooling ramps of the electron beam evaporator. Significant Ge concentration oscillation in the strained ^{28}Si layer can be observed for all configurations (I) - (III). However, the Ge concentration is non-vanishing in the concentration troughs (qualitative comparison to Si cap layer) and the difference between Ge-rich and Ge-poor is small,

indicating that the process is still dominated by Ge segregation during growth. The lowest Ge concentration was achieved in (I) where the growth temperature was lowest. Hence, we conclude that due to the surface roughening at lower temperatures, an improved structure can only be achieved with oscillating growth temperatures as well as low evaporation rates.

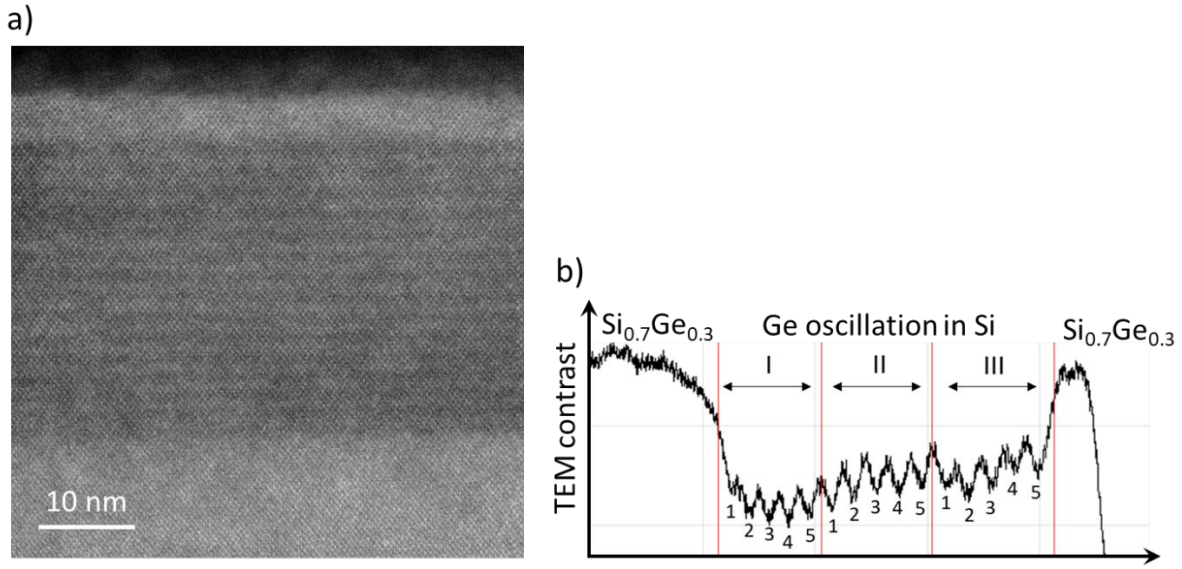

Fig. S1 (a) shows a cross-section TEM image of a test structure with 15 Ge oscillations in a strained Si layer on SiGe grown by MBE with a period length of 1.8 nm, where 5 oscillation were respectively grown with different shutter configurations. (b) depicts the TEM contrast the [0 0 1] growth direction.

2.2 Material Characterization Data from Heterostructures

The MBE grown heterostructures went through standard materials characterization, which include AFM roughness characterization, as well as X-ray diffraction (XRD) investigation. Hereby, Fig. S2 represents characterization of the heterostructure grown at 500°C and a) and b) show the AFM images of the as-grown heterostructure surface. The sample roughness on the respective 2x2 and 50x50 µm² area is 0.20 and 1.9 nm, respectively. The large scale area shows a pronounced cross-hatch pattern. Fig. S2 c shows a 113 reciprocal space of the heterostructure, proving the existence of a pseudomorphic strained Si QW layer on SiGe. d) shows a larger scale STEM image of a cross-section, indicating lateral homogeneity on several 100 nm scale.

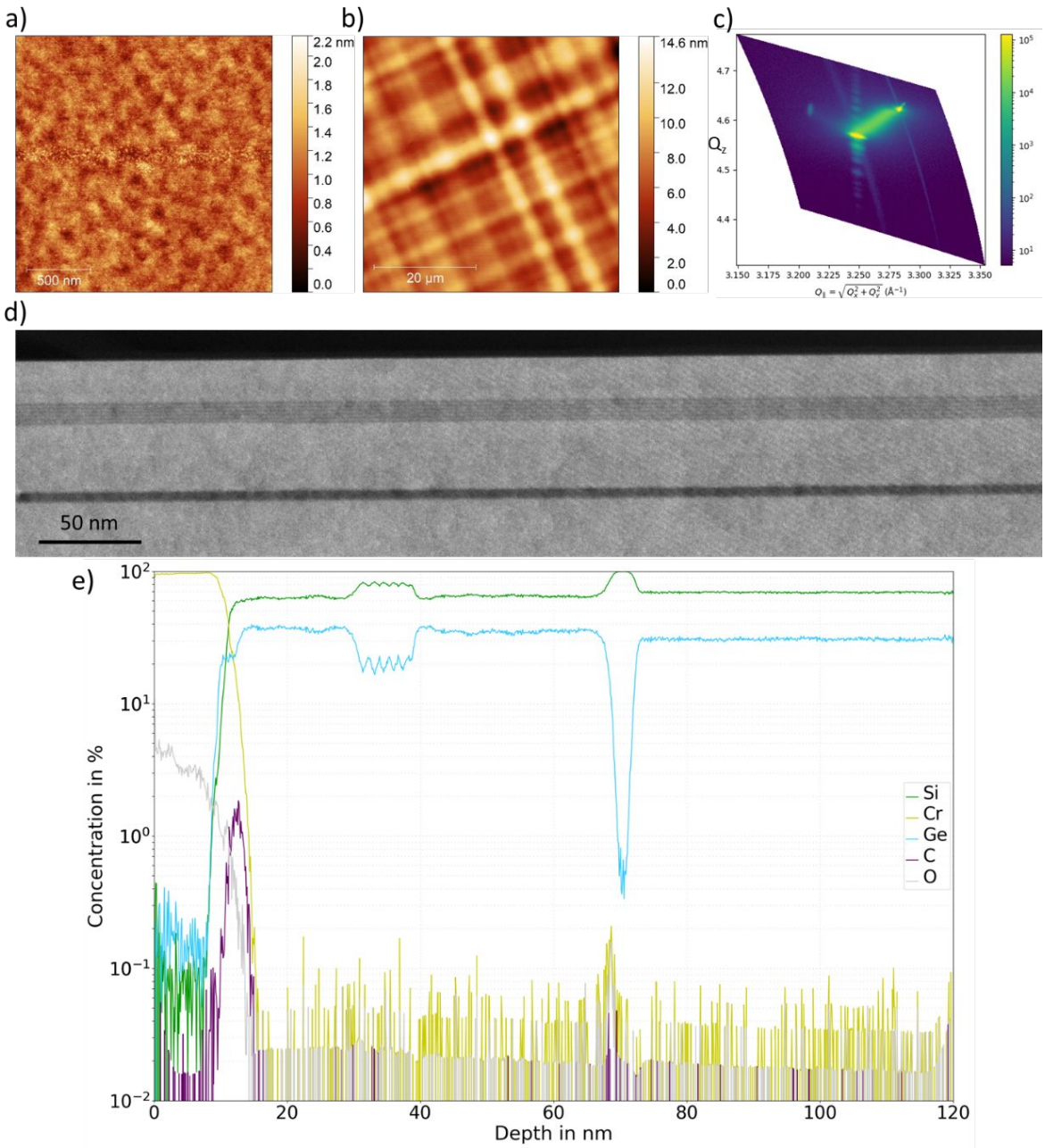

Fig. S2: a) and b) depicts AFM images of the as-grown surface of the heterostructure grown at 500°C on a 2x2 and 50x50 µm² area, respectively. c) shows a 113 reciprocal space map of the samples, d) shows a larger scale cross-section STEM image, and e) atomic concentration of Si, Ge, C, and O by APT.

AFM and STEM images of the sample grown with oscillating growth temperature is shown in Fig. S3. Hereby, the AFM roughness on the 2x2 and 50x50 µm² area shown in Fig. S3a and b is 0.22 and 1.9 nm, respectively. Slightly higher than growth at 500°C. The STEM image in Fig. S3c indicates lateral homogeneity.

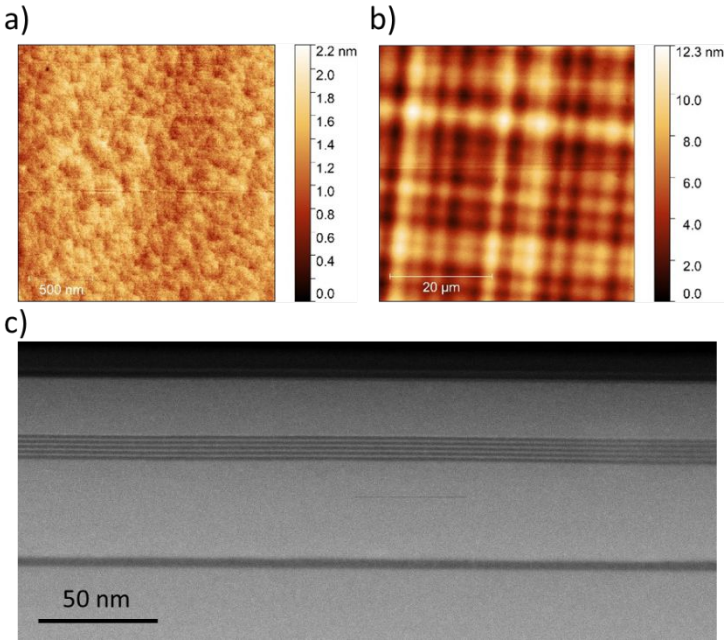

Fig. S3: a) and b) depicts AFM images of the as-grown surface of the heterostructure grown with oscillating growth temperature on a 2x2 and 50x50 µm² area, respectively. c) shows a larger scale cross-section STEM image.

2.3 Simulation - Robustness of the enhanced valley splitting

We demonstrate the robustness of the E_v enhancement due to the oscillating Ge concentration by means of various well designs in Fig. S4. The wells are built by periodically repeating the Ge distributions with P = 1.76 nm shown in Fig. S4a between the SiGe barriers. The corresponding theoretical E_v are highly enhanced with respect to evenly distributed Ge atoms indicating that the enhancement works as long as the periodic arrangement is present. The details of the profile (such as the height of the Ge peaks) can then further enhance the valley splitting.

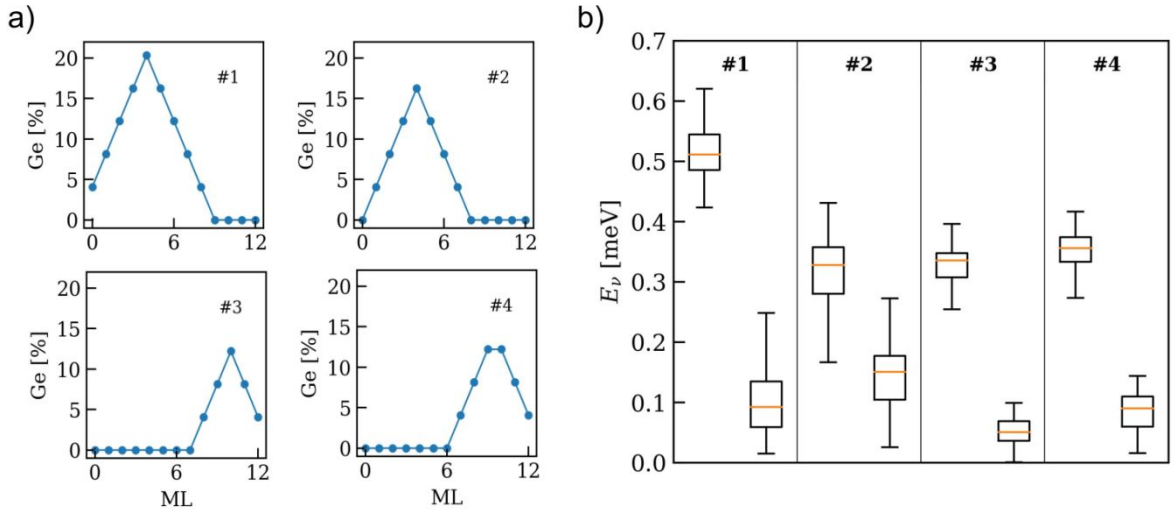

Fig. S4: Impact of various periodic Ge patterns that are periodically repeated in the quantum well of the TB simulation cell. a) Periods with various peak heights and peak shapes. b) Associated TB valley splitting (left box) compared to the equivalent Ge amount distributed evenly across the well. The valley splitting values are highly enhanced as long as the periodicity is present, while the exact shape is secondary.

Flaws in the Ge profile have been observed as a result of both growth techniques, with and without temperature modulation, see the ADF-STEM images of the heterostructures in Fig. 3 of the main text. As depicted there, a residual Ge content appears all across the quantum well. Thus, in addition to the simulations shown above, we present results for wells with flattened minima and maxima as well as residual Ge in the well. The results in Fig. S5 show still a clear enhancement of the valley splitting, which is qualitatively robust to changes of the details of the oscillating Ge profile.

In addition, we calculate the theoretical valley splitting for the heterostructure grown at constant temperature (from Fig. 3a). The Ge profile oscillates with an amplitude of 5% on top of a 22% Ge background. Despite the small periodic modulation, the enhancement of the valley splitting due to the oscillating Ge is clearly apparent.

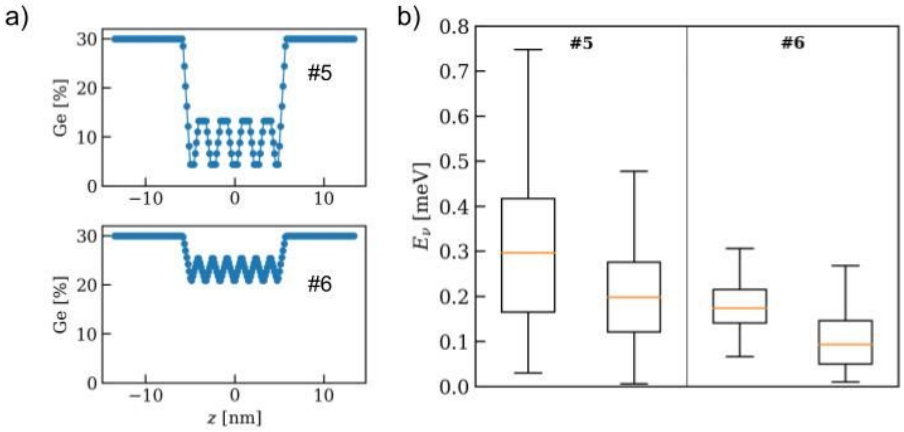

Fig. S5: Impact of periodic Ge profiles with a residual Ge content in the quantum well of the TB simulation cell. a) and b) show Ge profiles with cut-off peaks and residual Ge content, representing the characterization data from Figure 3c and 3f, respectively. The associated TB valley splitting (left box) is compared to the valley splitting for a well with an equivalent amount of Ge evenly distributed across the well (right box).

2.4 Convergence with respect to lateral cell size

The median values as well as the spread due to atomic fluctuations depends strongly on the lateral cell size. The median value is converged for a supercell with 24 conventional Si unit cells in x and y direction. Smaller cells lack the ability to accurately reproduce the desired Ge profile. Due to the limited number of atoms per monolayer, the realizable Ge content is bound to discrete values. For instance, each monolayer in a 3x3 supercell consists of 18 atoms which leads to discrete steps of 100/18% = 5.5%. The convergence of the median values is shown in Fig.S4a.

On the other hand, the spread of the valley splitting distribution is determined by the lateral extent of the supercell. Probing the interface with a more extended wave function indeed results in narrower distributions of E_v because the atomic fluctuations (alloy disorder), which cause the spread, average out. We characterize the spreads by the 25 to 75 percentile ranges obtained from our simulations as indicated by the boxplot in Fig.S4a. The decrease of the interquartile range (IQR) with respect to the number of unit cells N follows a 1/N trend as shown in Fig.S4b.

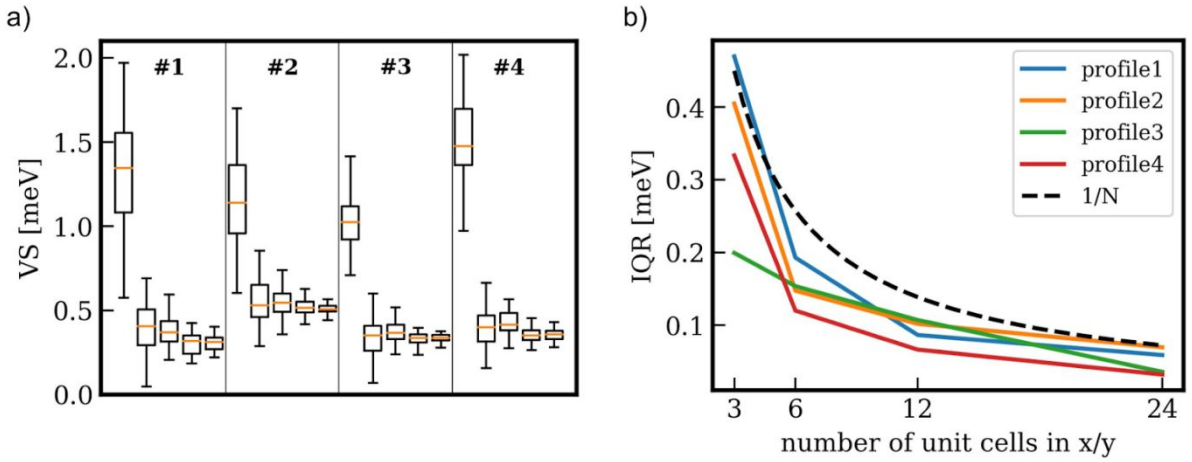

Fig. S4: Convergence of the valley splitting with respect to the cell size. a) The median value of E_v (orange line) for the four profiles of Fig. S2 as a function of the cell size. For each profile, we show results of the TB calculations for supercells with 3x3, 6x6, 12x12, 24x24 and 48x48 conventional Si unit cells (from left to right). In all examples, the median values are well converged for 24x24 unit cells. b) The 25 to 75 percent interquartile range (IQR) decreases with 1/N, where N is the number of unit cells in x and y direction.